3

Tribological Properties of Fluorinated Amorphous Carbon Thin Films

Miguel Rubio-Roy, Carles Corbella, José-Luís Andújar, Enric Bertran
Universitat de Barcelona
Spain

1. Introduction

1.1 Amorphous carbon characteristics

The peculiar electronic configuration of carbon atoms, $1s^2\ 2s^2\ 2p^2$, and the small energy difference between their 2p and 2s orbitals, compared to the binding energy of the carbon bonds, allow the electrons to rearrange in s and p mixed orbitals that enhance the binding energy with other atoms. This process is called hybridization and produces three different types of orbitals: sp = s + p, sp^2 = s + p + p and sp^3 = s + p + p + p.

Each different bonding state corresponds to a certain structural arrangement: sp bonding gives rise to chain structures (with two σ bonds and two π bonds), sp^2 bonding conforms onto planar structures (three σ bonds and one π bond) and finally sp^3 bonding produces tetrahedrical structures (four σ bonds). The p orbitals that form π bonds overlap less than the orbitals forming σ bonds. The reduced overlapping makes π bonds weaker than σ bonds. However, a number of scenarios are possible. Sometimes, as in ethene (C_2H_4), a σ and π bond combine producing a stronger bond between carbon atoms. This is called a double bond: C=C. Triple bonds consist of a σ bond and two π bonds, as in ethyne (C_2H_2). Although chemically stronger thanks to double bonds, the mechanical stability obtained with sp^2 hybridization in solids is limited, due to the planar geometry. Instead, sp^3 hybridization allows the creation of a three dimensional network of σ bonds.

Due to this variety of possible bonding configurations, carbon has a number of allotropes: graphene (sheet of sp^2 bonded carbons: σ bonds plus delocalized π bonds), carbon nanotubes and fullerenes (graphene sheets rolled over themselves forming cylinders or spheres, respectively), graphite (Bernal stack of graphene sheets), diamond (network of sp^3 bonded carbons) and amorphous carbon (cross-linked and non-organized carbon matrix with a mixture of sp^2 and sp^3 bonds). It is to the modification of the latter with fluorine that this chapter is devoted to.

The International Union of Pure an Applied Chemistry (IUPAC) defines amorphous carbon as "A carbon material without long-range crystalline order". It also states that "Short range order exists, but with deviations of the interatomic distances and/or interbonding angles with respect to the graphite lattice as well as to the diamond lattice."

Depending on the ratio of sp^2 and sp^3 bonds in the matrix, amorphous carbon (a-C) presents a variety of well-reviewed mechanical properties [Silva, 2003]. Tetrahedral amorphous carbon films (ta-C or TAC) present the highest hardness, with a high degree of sp^3 bonding and without hydrogen. It is almost exclusively deposited by filtered cathodic vacuum arc

(FCVA), [Martin et al., 1988; McKenzie et al., 1991; Fallon et al., 1993; Polo et al., 2000] although other techniques such as mass-selected ion beam (MSIB) [Kaukonen & Nieminen, 1992; Miyazawa et al., 1984] or laser deposition [Scheibe & Schultrich, 1994; Voevodin & Donley, 1996] can also be used. For the hydrogenated version of ta-C, plasma beam source (PBS) [Weiler et al., 1996] and electron cyclotron wave resonance (ECWR) [Morrison et al., 1999] have been used. Despite the high resemblance of ta-C to diamond on its short range microstructure and mechanical properties, its optoelectronics properties are controlled by the small percentage of sp^2 electrons with energies close to the Fermi level. [Silva, 2003]

On the other hand, films with comparable degrees of sp^3 bonding but soft are named polymer like carbon (PLC). These films have high H content (above 40%), which terminates single bonds and therefore reduces carbon-carbon cross-linking. The quantity of sp^3 bonds is high due to hydrogen's preferential bonding to carbon in sp^3 configuration, but this is no longer related to enhanced hardness. This kind of films present a small amount of defects compared to others and have a wide bandgap [Silva et al., 2002].

Films with intermediate hydrogen content can be either hydrogenated ta-C or hydrogenated a-C (a-C:H). The latter is the most studied type of a-C films and has been known in the literature as diamond-like carbon (DLC). It is softer than ta-C(:H) but still harder than most materials: values ranging from 20 to 40 GPa. Density is also slightly smaller than that of ta-C(:H). Its main advantage is the simple setup for its deposition. A wide range of deposition techniques is available compared to the complex setup for ta-C deposition [Aisenberg & Chabot, 1971; Zou et al., 1989; Koidl et al., 1990; Kessels et al., 1998]. Also, DLC has a wider range of optical gaps than ta-C depending on the deposition conditions, which enables it for applications such as UV nanoimprint molds, where middle or near UV light transmission is necessary. For shorter wavelengths, thin films allow to further extend the working range.

Figure 1 shows the space of film types depending on the sp^2:sp^3 ratio and H content. Figure 1a is an updated version of the popular diagram by [Ferrari & Robertson, 2000] which includes hydrogenated films. Figure 1b by [Silva, 2003] presents a revised diagram based on a wider review.

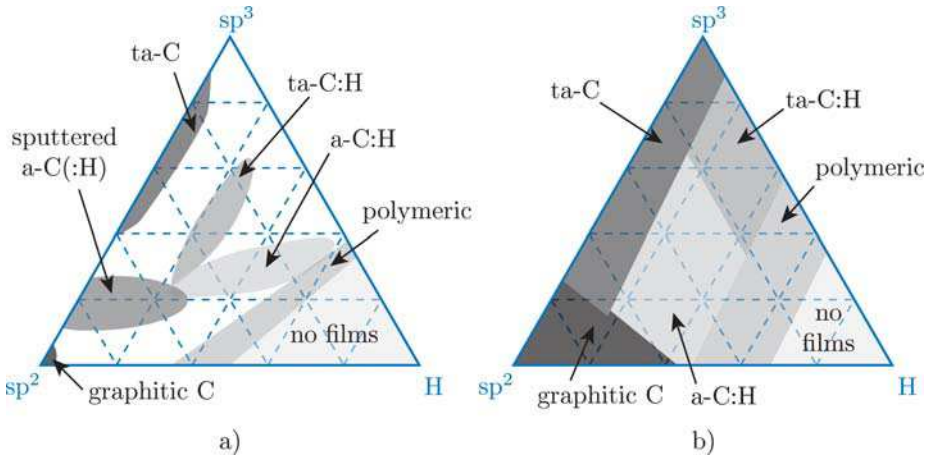

Fig. 1. Ternary diagrams of amorphous carbon types with respect to sp^2 and sp^3 fraction, and H content. a) by [Robertson, 2002]; b) by [Silva, 2003].

High hardness and elastic modulus are the main features of a-C:H and ta-C(:H) films. However, the rigid network of the films produces a high intrinsic compressive stress of up to 12 GPa [Ferrari et al., 2002]. This is an important drawback in the production of DLC coatings, since it limits the thickness depending on the adhesion to the substrate. For badly adhered or too thick films, cracks can appear and finally peel off the film if they progress, or otherwise dramatically reduce wear resistance. Thin buffer layers between substrate and film can be used to avoid this problem. Several transition metals and compounds can be used to this respect (W, Ta, TiC, Cr, SiC, etc.) depending on the substrate nature [Lee et al., 2000; Bahl et al., 2000; Kiuru et al., 2003].
With regard to surface properties, water contact angle has usually been examined providing relatively high values from 55° to 70°, depending on the presence of low energy C–H groups on the surface and the oxygen contamination of the film. The introduction of elements like F, Fe, Al and others has proven to be a useful method to increasing contact angle values up to more than 100° [Grischke et al., 1995; Chen et al., 2001].

1.2 Deposition methods

DLC can only be obtained at conditions far away from equilibrium, and so it is not spontaneously found in nature. The control of the growth parameters broadens the field of carbon microstructures and, in parallel, the properties of this material, which can only be synthesized in thin film form.
The production of a-C thin films is carried out by a large variety of deposition techniques. Some of them are adequate for laboratory studies while some others are more addressed to industrial production. Almost all processes work with low pressure of precursors or inert gases. Under these conditions, the increased mean free path of the species allows adequate particle energies, in order to obtain good mechanical and tribological properties. DLC films, and hard coatings in general, are very sensitive to particle bombardment during their growth. Therefore, this is a key parameter that must be controlled in any deposition method. Contamination by oxygen can affect importantly the properties of DLC. For this reason, clean processes in chambers capables of reaching low base pressures are used. The different methods to deposit DLC exhibit three characteristics [Silva, 2003]:

i. A plasma is used as the source of reactive species.
ii. The substrate is found, in general, at room temperature. At least there is no need to maintain a high substrate temperature during the process unlike in classical CVD processes.
iii. Energetic particles (ions and/or neutrals) participate in the deposition process.

Ion beam deposition

Ion beam deposition was the first method used for the synthesis of DLC [Aisenberg & Chabot, 1971]. Carbon and hydrocarbon ions coming from a graphite cathode are condensed in an energetic beam and produce sp^3 states as they impinge on the growing film. Ion beam sources operate efficiently within an ion energy range of 100—1000 eV. Mass selected ion beam (MSIB) techniques are addressed to obtain ion beams with a certain energy. Ions pass through a magnetic filter that selects charged species with a fixed charge to mass ratio. Unfortunately, the ion beam is usually weakly ionized and, thus the mechanical properties of DLC are not optimal.

Sputtering

Magnetron sputtering is a well-known physical vapor deposition technique (PVD). It is one of the most used techniques, in industrial environments, to grow DLC. The impinging

species are commonly sputtered from a graphite target, which is RF- or DC-powered, in an Ar glow discharge [Rubio-Roy et al., 2007a]. The energy of the ion species being deposited can be increased or adjusted by applying a DC bias to the substrate or by using an unbalanced magnetron whose magnetic field substantially reaches the substrate.
Reactive magnetron sputtering processes are also possible if hydrogen or hydrocarbon source gases are added to Ar. An alternative sputtering process can be performed without plasma: an Ar ion beam from an ion gun sputters a carbon target, say graphite, while another beam bombards the growing film to promote sp^3 formation. This method is called ion beam assisted deposition (IBAD).

Cathodic arc

Cathodic arc constitutes one of the oldest vacuum deposition techniques [Randhawa, 1988; Sanders & Anders, 2000]. The arc discharge is concentrated at the cathode surface, where high ion densities ($\approx 10^{12}$ A/m^2) form non-stationary spots. The ionization of species reaches 100% of the total flux, and the maximized parameter is the electron current to the anode, which is called arc current. The ion current is about 10—100 times lower than the arc current. This method is really appropriate to obtain hard DLC films, with a significant sp^3 fraction, but certain issues have limited its use. First of all, films may present serious inhomogeneities due to the instabilities caused by the location of the arcs in the cathode. Secondly, the installation of a filtering device is necessary to prevent the deposition of macroparticles. Filtered cathodic vacuum arc (FCVA) solves the last problem by means of a magnetic filter, either in single bend or S-bend configuration [Robertson, 2002].

Pulsed laser deposition

Pulsed laser deposition (PLD) provides energetic ions, as in cathodic arc processes. Therefore, it is possible to deposit DLC films with high sp^3 content with this technique, without the need of substrate biasing or great current discharges [Voevodin & Donley, 1996]. The intense energy pulses (15-30 ns) of a laser beam are able to vaporize a carbon target, which shows major advantages when it is graphite due to minimization of droplets emission. Fluxes of neutrals, ions and particulates are ejected from the target through an intense plasma, named plasma plume. The first PLD setups used Nd:YAG lasers, operating at a wavelength of 1064 nm. Nowadays, excimer lasers have progressively substituted them because higher-quality DLC is obtained using shorter wavelengths, for instance 193 nm and 248 nm (ArF and KrF lasers, respectively). The structures of DLC samples grown by PLD can be nanocrystalline diamond and ta-C.

Plasma-enhanced chemical vapor deposition (PECVD)

PECVD is a very popular technique to produce DLC films. A plasma is ignited in a reactor, between two electrodes of different areas, giving place to an asymmetrical discharge. The supplied power cannot be DC, since DLC may be electrically insulating. Thus, PECVD processes employ capacitively coupled RF power or pulsed-DC power. As depicted in figure 2, power is driven to the small electrode (cathode), where the substrate is placed, and the reactor walls are usually grounded (anode) [Rubio-Roy et al., 2007b].
The negative bias of the substrate cathode accelerates the bombarding ions to create sp^3 sites. The enhancement of ion-to-neutrals ratio in the discharge needs low-pressure plasmas, but too low pressures will avoid a self-maintained discharge regime. This appropriate equilibrium is accomplished by raising the supplied power or by coupling an external magnetic field to the sheaths. The latter is performed in inductively coupled plasmas (ICP).

Electron cyclotron resonance systems (ECR) use both microwaves and magnetic field for a resonant transfer of energy to the electrons in the plasma. The simultaneous use of two different plasma sources, besides increasing the ionization degree, permits to decouple the particle flux and the bombarding energy of the ions [Corbella et al., 2008].

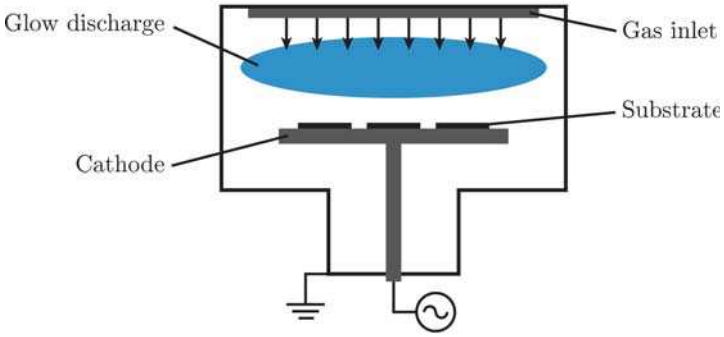

Fig. 2. Layout of a PECVD reactor.

Electron cyclotron wave resonance (ECWR)

When trying to couple low frequency electromagnetic radiation to a plasma, the latter behaves as a conductive medium and totally absorbs the incident waves within a characteristic absorption depth ("skin" depth). The plasma becomes transparent to the electromagnetic waves only when the excitation frequency exceeds the plasma frequency or when its conductivity is reduced (e.g.: with higher plasma density). However, RF excitation frequencies require very low plasma densities.
ECWR consists on applying a weak magnetic field (≈20 G) that inhibits plasma conductivity by confining electrons in cyclotron orbits around the field lines. Hence, the electromagnetic radiation can be distributed across the plasma, which contributes to increase the plasma density and generates propagating electromagnetic modes [Morrison et al., 1999; Rodil, 2000]. The dimensions of the chamber are set so that one of these modes matches the resonant condition.

1.3 Tailoring of amorphous carbon properties

DLC shows special surface properties, and in some cases, they must be tuned depending on the selected application. The physical and chemical properties can be tailored by adding new elements into the a-C matrix as nanocomposites or by structuring the material in multilayers or gradient coatings. This provides the so-called modified a-C. Another strategy consists on patterning its surface, as explained in section 3.1.
Regarding the mechanical properties of DLC, both hardness and elastic modulus reach high values, and can be tailored by controlling the sp^3 fraction and hydrogen content, if any. Although hardness of a-C:H ranges from 20 to 40 GPa, the rigid network of the films provides an intrinsic compressive stress ranging from 0.5 to 12 GPa. This high stress is an important drawback in the production of DLC coatings, since it limits the film thickness to less than 1 μm. In fact, the accumulation of micro-strains within the amorphous matrix leads to a global compressive stress that is large enough to damage the film by development of cracks and strains that prevent the adhesion to substrates and reduce film stability. DLC

films, deposited by RF-PECVD, thicker than 50 nm are generally so stressed that they lose their consistency and delaminate.
Besides improving adhesion to substrate, another strategy to avoid film peeling is stress relaxation. This is possible through doping with N, Si or metals, as well as by post-annealing or incorporation of nanometric particles (DLC nanocomposites), but these operations may degrade the mechanical properties [Zhang et al., 2002; Chen & Hong, 2003; Corbella et al., 2009a]. Metal incorporation in a DLC matrix has been proved to reduce stress below 1 GPa and maintain hardness and wear rate within acceptable values [Dimigen et al., 1987]. Low stress values are also achieved by depositing alternating hard and soft a-C layers [Ager et al., 1997; Logothetidis et al., 2000]. The resulting multilayered structures show a lower overall stress, and hardness is almost unaffected. Metal and a-C multilayers (Me/a-C) [Bertran et al., 2003], as well as a-CN/a-C structures [Pino et al., 2001], have been also deposited with similar results. Bias-graded deposition of DLC provides the best tribological performance through surfaces showing high sp^3/sp^2 ratios, which gradually decrease from the surface to the interface in order to enhance adhesion [Zhang et al., 2004]. Another way to improve coating adhesion consists in growing a buffer layer (Ti, Cr) prior to DLC deposition. Figure 3 summarizes the above mentioned strategies.

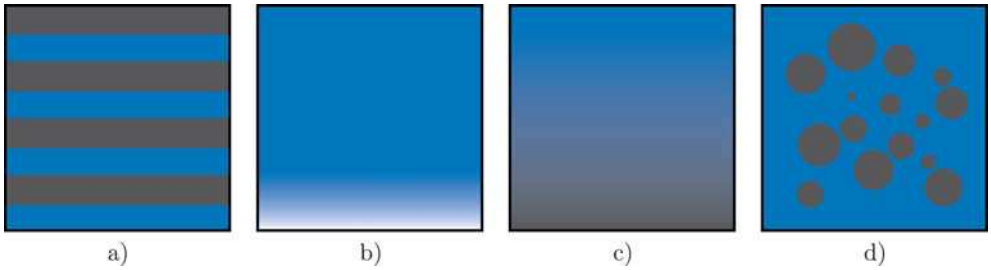

Fig. 3. DLC modified structures: a) multilayers; b) buffer layers; c) composition-graded coatings; and d) nanocomposites.

DLC films with hydrogen are mostly exploited in tribological applications due to their low friction coefficient and low wear rate. In all environments, the tribological behavior of DLC is controlled by an interfacial transfer layer formed during friction [Voevodin et al., 1996]. Thus, DLC is a valuable alternative as solid lubricant for applications where liquids are not convenient.
Besides wear and corrosion resistant, DLC is also known to be a hydrophobic material. The C–H groups located on the surface diminish the wettability, which is parametrized by the contact angle held between a liquid drop and the film surface. DLC typically exhibits a contact angle of 55–75° for water, although it can be increased by adding metals such as Fe or Al. In the case of Al-DLC, the contact angle exceeds 100° [Chen et al., 2001]. The high hydrophobicity shown by a-C:H:Si:O and a-C:H:F films is also advantageous for anti-sticking and self-cleaning applications [Grischke et al., 1998; Rubio-Roy et al., 2007b]. Highest values of contact angle are reached when combining hydrophobic films together with special surface architectures [Kim et al., 2007]. On the other hand, a-C:H:Si:O films find also applications as ophthalmic and decorative coatings due to their comparatively high optical transmittance. The resistance to higher temperatures makes a-C:H:Si ideal as protective coating in components for thermal processes.

Low roughness is another intrinsic surface property that makes DLC films suitable for certain tribological applications. DLC layers show a flat and smooth surface, with their roughness being minimized when deposited by filtered arc evaporation. RMS surface roughness below 0.05 nm has been reported for DLC deposited either by sputtering or PECVD [Peng et al., 2001]. These atomically flat surfaces show improved tribological properties of importance for applications such as hard drive disk coating. Moreover, surface roughness of ultra-thin DLC films is revealed to follow fractal scaling laws, i.e. it is related to film thickness through an exponential function [Casiraghi et al., 2004].

1.4 Applications

The wide variety of applications of DLC is mainly addressed to hard coatings with special tribological properties. These properties can be tuned by modifying DLC structure and by incorporating other elements [Hauert & Patscheider, 2000], whereas other properties ensure its performance as optical filter or for components with electronic functionality.

The fastest growing market for DLC application during the previous years was the automotive industry [Lampe et al., 2003], in which DLC, ta-C, W-DLC and WC/C multilayers were being preferentially developed as hard and tribological coatings [Hauert, 2004]. Automotive industry demands solutions for preparing low friction and wear resistant coatings for lubricant performance on components. DLC fulfils these requirements and has been tested on a large number of automotive components: gears, wrist pins, valve filters and fuel injector parts. Specifically, serial production of metal-containing DLC (Me-DLC) coatings by physical vapor deposition has been performed on diesel injection systems [Gahlin et al., 2001]. The modern high-pressure injection systems were developed thanks to DLC. Also, racing cars were the first targets in automotive applications of DLC, where it was used to maximize engine power by friction reduction [Johnston & Hainsworth, 2005].

The combination of elevated hardness and wear resistance of DLC is appropriate for cutting and abrasive wear instruments, like drills and other machines used in material manufacturing. Optimal frictional properties of DLC coatings increase efficiency and lifetime of ultrasonic motors (USM), which have applications in robotics and automation equipments [Ko et al., 2005] where liquid lubricants are not an option. Also, dry lubricants are indispensable for pharmaceutical and food processing systems because of requirements of chemical inertness and low friction. In this way, any machine component is protected by DLC: worm gears, lead screws, roller bearings, compressors and air bearings. Concerning textile industry, the existence of residual substances and adding compounds in yarn motivate the coating with DLC of components of textile machines in contact with yarn, e.g. spinning rings, rapiers and needles. Anti-sticking properties of DLC are used to obtain better product quality in injection molding. Gillette Mach3 blade edges constitute a successful application of ta-C. These edges, coated by 150 nm thick DLC, appeared in 1998 and consolidated razor blades as one of the basic applications of this material.

DLC and modified DLC present elevated hydrophobicity, which is a basic requirement for surfaces of fluid-contacting components and devices. This material is useful to improve surface properties of inner walls of pipes and tubes. Presently, extensive research is being carried out to use DLC as gas barrier on the inside surfaces of bottles and packaging due to its high atomic density [Chhowalla, 2003; Abbas et al., 2005; Ozeki et al., 2009].

DLC coatings are applied in optical storage devices in order to protect the disk. The main conditions are low wear rate and transparency in the recording wavelength and low deposition temperature to allow the use of polymeric substrates.
The high transparency in the infrared (IR) range makes DLC suitable for surface-protection applications in IR optics [Rusliet al., 2003]. In the visible range, sunglasses from Ray-Ban and glass plates for laser barcode scanner windows demonstrate the performance of DLC as scratch resistant coating for light transmitting surfaces [Hauert, 2004]. The control of interferential colors suggested DLC films for their use as decorative coatings. Electroluminescent and phase-shifting are other applications of DLC.
Protection to corrosion and wear of magnetic hard disks is one of the most widespread uses of ultra-thin DLC coatings [Morrison et al., 1999; Bhushan, 1999]. They must be ultra-thin to minimize the gap between the disk and the recording head, to achieve the highest areal storage densities. Magnetic media are currently protected by an approximately 2 nm thick DLC overcoat. Atomic smoothness (<0.15 nm) and absence of pinholes are of importance in order to protect the disk from corrosion [Jiang et al., 2010; Casiraghi et al., 2004].
Current research on DLC or modified DLC is mainly motivated by its biocompatibility [Grill, 2003; Hauert, 2004; Roy & Lee, 2007; Ma et al., 2007]. This property, together with antithrombogenicity, makes DLC-based films special candidates for medical applications where wear-resistant coatings, such as in prosthesis, are required. The surfaces of the implants are exposed to body cells and fluids, and are also exposed to potentially corrosive medium. These effects can provide cellular damage, infections, blood coagulation and failure of the implants. Coating the implants with protective films, which can reduce corrosion and wear, may extend the lifetime of implants by preventing or alleviating the aforementioned issues. Further biomedical applications include surgical tools and other devices in contact with blood or organic tissues [Dearnaley & Arps, 2005].

2. Modification with fluorine

2.1 Fluorine incorporation

In addition to metals, the introduction of Si, O, N or F in a-C films has also been investigated. In this case, O and N increase the surface free energy (SFE), while Si and F reduce it. Interestingly, addition of both Si and O can reduce the SFE more than only with Si [Grischke et al., 1995]. Among these elements, fluorine incorporation exhibits the highest water contact angles (higher than 100°) and the lowest surface energies (about 20 mJ/m^2).
A number of recent studies regarding the introduction of F in DLC films (FDLC) can be found in the literature. However, one must distinguish between growing fluorinated films and fluorinating films or other surfaces. The former corresponds to the growth of films containing fluorine in bulk, while the latter only adds fluorine functionalization to the surface. This chapter focuses on the growth of fluorinated films.
Fluorination of surfaces is easily achieved by etching with common fluorocarbon plasmas. This consequence has sometimes been seen as an adverse effect and cleaning procedures have been designed to remove fluorinated groups from the surface [Simko et al., 1991]. Others have intentionally used fluorocarbon plasmas to functionalize surfaces [Miyamoto et al., 1991; Korotkov et al., 2007; Roy et al., 2007].
The advantage of growing fluorinated films is that even after being worn out to some extent, the new surface preserves bulk's chemical composition. In addition, fluorine not only changes surface properties but also provides interesting bulk properties. Fluorinated

amorphous carbon has been extensively studied as a low dielectric constant (low-κ) material for electronic devices where parasitic capacitance must be avoided, because it can be deposited with microelectronic compatible methods. Static dielectric constant values as low as 2.1 have been obtained by RF-PECVD with CH_4 and CF_4, with increasing ε_r with RF power [Endo & Tatsumi, 1995]. As a comparison, the traditional dielectric layer in microelectronics, SiO_2, has ε_r = 4.0 and current dielectrics used in 90 nm, 65 nm and 40 nm lines of Intel® processors have ε_r = 3.0 [Grill, 1999]. The other major property of fluorinated amorphous carbon is its reduced surface energy. Compared to Si, fluorine not only reduces its polar component but also the dispersive contribution. The introduction of fluorine in the film displaces hydrogen, and bigger $-CF_2$ and $-CF_3$ groups are formed. This reduces the network density therefore reducing the dispersive component [Grischke et al., 1995]. When the appropriate growing conditions are used, low surface energy coatings (20 mJ/m²) with improved hardness (5 to 20 GPa) over PTFE (18 mJ/m² and 0.3 GPa) can be obtained. These conditions are reported to fall into the moderate fluorination conditions ($R_F^{film} \equiv [F]/([F]+[C]) < 0.2$) [Donnet, 1998].

The deposition process of fluorinated a-C films is usually performed by PECVD although sputtering has also been used in some studies. The deposition by sputtering can be performed in reactive mode by using a graphite target and some fluorocarbon gas (e.g. CF_4, CHF_3, etc.) [Trippe et al., 2004; Jiang & Ning, 2006; Guerino et al., 2007] or by directly sputtering a PTFE target [Gonon & Sylvestre, 2002; Tang et al., 2005].

Instead, more work can be found in the literature about PECVD. There is a number of possible precursors with different C:F ratio which can be used to deposit fluorinated amorphous carbon. As reported, film's fluorine content is primarily determined by the gas precursor chemistry. Generally, more fluorine in the process gas results in higher fluorine concentration in the film; adding hydrogen to the feed gas reduces the film F:C ratio [Mountsier & Samuels, 1998]. CF_4 is one of the highest F:C ratio precursors available. Combined with CH_4, it is reported to produce lower dielectric constant than other precursors, and Vicker's hardness values from 5 to 10 GPa [Jacobsohn et al., 2000]. Other studies, show results for the same gases with hardness values from 16 to 19 GPa and surface free energy values descending from 40 mJ/m² for films deposited from pure CH_4 to about 28 mJ/m² for 4:1 CF_4:CH_4 gas flow ratio [Yu et al., 2003].

The results presented in this chapter were obtained using CHF_3, a barely studied gas for PECVD processes. Only a few papers, concerning deposition of low-κ dielectrics, can be found in the literature and diamond-like properties have virtually not been sought with this precursor. Among them, an article from Winder and Gleason shows lower roughness values and higher fluorine incorporation for films deposited from CHF_3 than $C_2H_2F_4$ or CH_2F_2 [Winder & Gleason, 2000]. Xin et al. have also published work about growth of a-C:F:H films deposited with CHF_3 and using ECWR-PECVD. Neither the mechanical properties nor the surface energy of the films were examined [Xin et al., 2003].

However, more work can be found dealing with the use of CHF_3 as precursor for plasma treatments, including treatments of previously grown DLC films [Kawasaki et al., 2004]. Schvartzman and Wind make use of the modified DLC for NIL molds and show slightly lower surface free energy values for surfaces treated with CHF_3 than with C_4F_8 [Schvartzman & Wind, 2009].

2.2 Surface and chemical properties of FDLC

X-Ray Photoelectron Spectroscopy (XPS) [Goldstein et al., 1992] is an adequate technique to quantify fluorine to carbon ratio in the films, although it is not able to detect hydrogen. The analyzed films always show lower F to C ratio in the film than in the precursor. For example, for films deposited with pure CHF_3, F to C ratio in the gas is 3 while in the film is one. The results of F:C ratio in the film are shown in figure 4 as a function of $R^{gas}_{CHF_3} \equiv \Phi_{CHF_3}/(\Phi_{CHF_3}+\Phi_{CH_4})$, where Φ_x represents the gas flow of x.

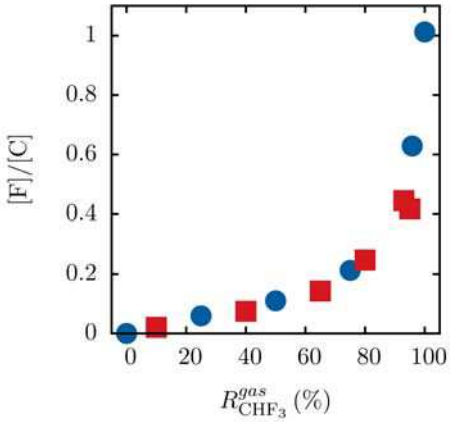

Fig. 4. Atomic F to C ratio in the film as determined from XPS analysis for two series of samples (deposited with 10 sccm of total gas flow, red squares; and 25 sccm blue circles).

The diamond-like characteristics of the films for low $R^{gas}_{CHF_3}$ suggest that the growth mechanism is ruled by the subplantation model [Robertson, 2002; Lifshitz et al., 1989, 1990, 1994]. Under these conditions, there is an intense energetic ion bombardment which subplants energetic species, either locally increasing stress (according to McKenzie et al. [McKenzie et al., 1991]) and stabilizing diamond-sp^3 phase, or by locally increasing density which would tend to increase sp^3 bonding as well (according to Robertson [Robertson, 1993]). In any case, ion bombardment causes the loss of hydrogen and fluorine from the surface and subsurface.

Ion bombardment is carried out by positively charged species that are accelerated in the plasma sheath towards the sample. At low $R^{gas}_{CHF_3}$, fluorine (and probably hydrogen) incorporation into the film is low while for low methane concentrations the F:C ratio rises significantly. The high hydrogen content provided by CH_4 probably etches away fluorine atoms back to the plasma, which fits with optical emission spectroscopic actinometry results, from the plasma, for atomic F. For a-C:H films, it is believed that atomic H, either neutral or ion, reacts with C–H bonds, abstracting H and creating H_2. According to these results, when fluorine is added, atomic H probably reacts with F in the film, as well, creating volatile HF.

As $R^{gas}_{CHF_3}$ is increased, hydrogen introduced as part of the feed gas is reduced and, eventually, fluorine content in the films starts to increase. Therefore, the reduction of atomic hydrogen increases the chances of fluorine to remain in the film. Fluorine, the substitute of

hydrogen when $R^{gas}_{CHF_3}$ is increased, does not produce the same effect as H, due to its strong electronegativity, therefore avoiding the bombardment of F atoms. In addition, ion energy measurements have shown that the progressive substitution of CH_4 by CHF_3 reduces, and finally eliminates, the population of high energy ions [Corbella, 2009b]. The combination of hydrogen reduction, exchange by a strong electronegative atom (F) and reduction of the density of energetic ions bombarding the growing surface, would explain the non-linear increase of [F]/[C].

2.3 Friction of FDLC

Several factors influence the frictional behavior of DLC thin films: the degree of sp^2 or sp^3 carbon bonding, the amount of hydrogen in the film, the eventual alloying elements, the chemical and mechanical interactions between film and ball, the ball composition or the film and ball roughness [Erdemir & Donnet, 2006]. Moreover, the sliding conditions of speed and load [Heimberg et al., 2001] or debris production can also determine the possible interactions in the experiment. The interpretation of friction data is therefore not straightforward.

The results presented in this section correspond to measurements carried out with a nanotribometer (50 mN load) in a controlled N_2 + H_2O atmosphere as detailed elsewhere [Rubio-Roy, 2009].

Measurements show that friction coefficient is reduced for increasing relative humidity (RH) between 20% and 60%. Beyond that point, it does not suffer significant variation. Moreover, for high RH, friction does not seem to depend on the fluorination degree of the films. Regarding the effect of fluorine introduction, non-fluorinated films provide, on average, the lowest friction, while films deposited with $R^{gas}_{CHF_3} = 10\%$ show the highest friction (0.4 for 20% RH). For higher F concentrations friction coefficient is reduced again. Low-fluorinated films see their friction more affected with humidity than non-fluorinated or highly-fluorinated DLC films.

Optical microscope photographs (see figure 5b) show fiber-like debris particles at both sides of the sliding track. This phenomenon occurs when discontinuous wear is given contrary to what happens when a transfer layer is present between the sliding counterpart and the film surface [Erdemir & Donnet, 2006].

Hydrogen terminated surfaces provide low friction characteristics due to the passivation of σ and π carbon bonds on the surface [Erdemir & Donnet, 2006]. As the WC ball slides over the surface, H atoms are mechanically removed from the film by strain effects thus leaving superficial dangling bonds [Li et al., 2005]. Depending on the experimental conditions, and specifically on the gas environment, hydrogen and hydroxyl groups originated from water will passivate these bonds again. In our experiment, for RH between 20% and 60% the results would justify this casuistic, so that bonds would react with water to restore themselves to a low energy state. However, for higher presence of water (from 60% to 80%), friction is stabilized for all films and independently of humidity or fluorine content (see figure 6). For these values of RH, a layer of physisorbed water could be formed on the surface, as already suggested by other authors [Erdemir & Donnet, 2006; Erdemir, 2001], which would make friction independent of the films' variations.

Regarding the rather high friction values for $R^{gas}_{CHF_3} = 10\%$ in comparison to the rest, this behavior could be due to at least two competitive mechanisms. One of them would be the

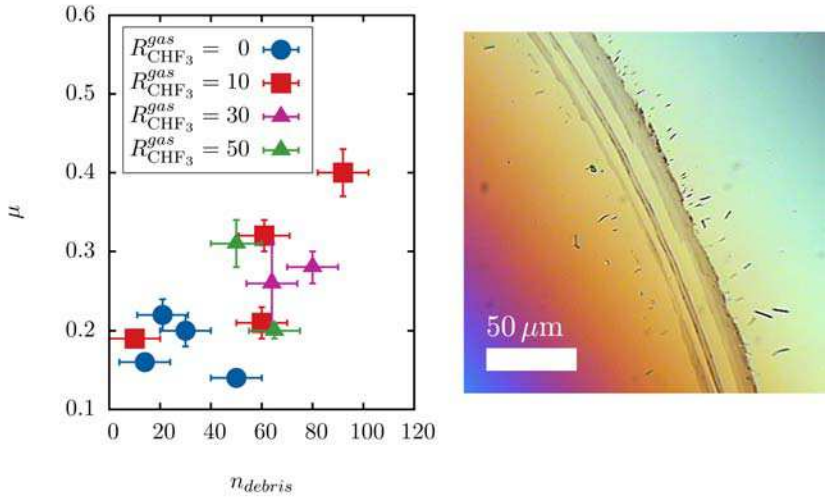

Fig. 5. a) Friction vs number of debris particles visible at 50× (200×200 μm).The dependence of friction with number of particles is only clear for high friction values; b) 50× optical microscope picture of a typical sliding track, corresponding to a film with $R^{gas}_{CHF_3} = 10\%$ measured CHF_3 at 60% RH. Fiber-like debris particles are present at both sides of the sliding track.

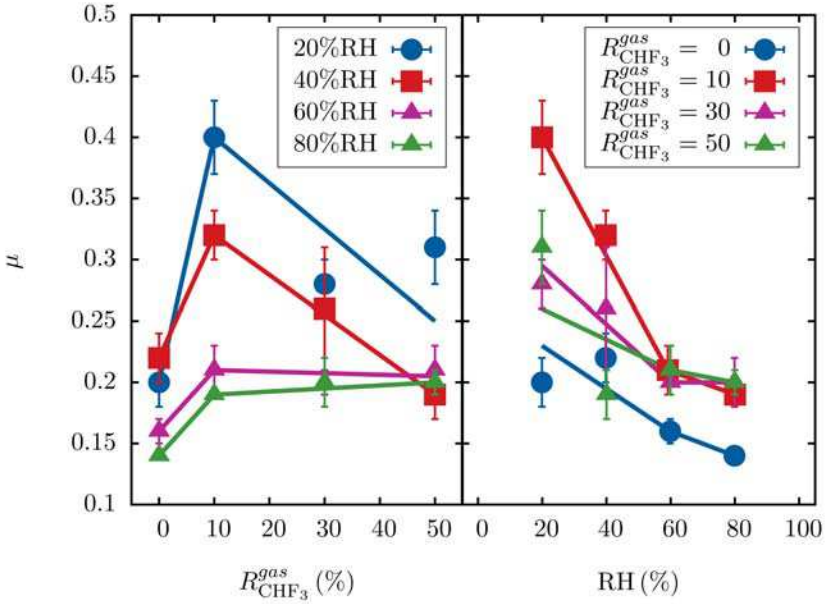

Fig. 6. Friction dependence on humidity and fluorination degree.

somewhat beneficial effect of F presence to reduce friction by reducing adhesion to the sliding counterpart and by passivating carbon with a high-energy bond. The other would be the disadvantageous effect of a lower C atomic density (F is bigger than H), the reduced reservoir of H inside the film that would otherwise relink dangling bonds on the surface, and the probable decrease of H in the film as expected from the reduction in hydrogenated species in the plasma, from optical emission spectroscopic actinometry. The increase of friction with fluorine for humidity values below 40% is in agreement with other analogue works [Gilmore & Hauert, 2001].

The statistical analysis of 50× micrographs, taken after the tests, reveals that the influence of debris production in friction must also be taken into account as friction increases, where a stronger correlation between debris and friction is found. However, for low friction experiments, debris influence is limited and strongly coupled to microscopic effects (tests with similar debris production have different frictions and the other way round).

Films' roughness (as measured from atomic force microscopy) is sufficiently low so that it is a minor factor in friction phenomena for the tested $R_{CHF_3}^{gas}$ range), not producing interlocking and/or asperity-asperity interactions during sliding.

2.4 Abrasive wear of FDLC

Abrasive wear measurements were carried out with a 1:3 suspension of alumina particles 1 μm in diameter in glycerin. Such setup is highly hygroscopic and minimum changes in ambient humidity can affect the results. All measurements must be done during a short period of time (to avoid water absorption) and at a controlled temperature and relative humidity (here 23°C and 33%).

CSM Calowear equipment was used to measure the abrasive wear resistance of the amorphous carbon films. The measurement setup consists on a plastic or hardened stainless steel ball leaning against the surface of interest (which is tilted a known angle) and spun by a rotating shaft at a known distance from the surface. As the ball center does not move relatively to the surface, the footprint of the test is very small. More details about the setup can be found elsewhere [Gee et al., 2003].

Two different balls with equal diameter were used to test the wear resistance: a steel ball applying a force of 0.54 N and a plastic (polyacetal) ball producing 0.092 N of normal load.

The deposited films showed high wear resistance up to $R_{CHF_3}^{gas} = 80\%$ (see figure 7), with values in the range of 0.2×10^3 μm³/Nm to 0.4×10^3 μm³/Nm, one order of magnitude more resistant than monocrystalline Si (100) in the same conditions (2.1×10^3 μm³/Nm). Fluorine content slightly increases wear rate, which is consistent with the observed changes in composition. The overall stability of the films is excellent. Data in figure 7 at $R_{CHF_3}^{gas} = 10\%$, 40%, 60% and 80% correspond to two-year-old films, in contrast to the rest of data, which corresponds to recent (weeks old) films. Contact angle measurements also confirm the stability of the films.

For more fluorinated films, this setup worn the film too much, so that the rate could not be measured. This is probably a consequence of both the reduced cohesive forces of the films and a loss of adhesion between film and buffer layer.

However, using the plastic ball during shorter periods of time, it could be determined that fluorinated films are up to 5 times more resistant than Si up to $R_{CHF_3}^{gas} = 80\%$. Beyond that point, Si is more resistant, which evidences either a dramatic reduction of adhesion between film and buffer layer, or a strong structural and chemical change of the film.

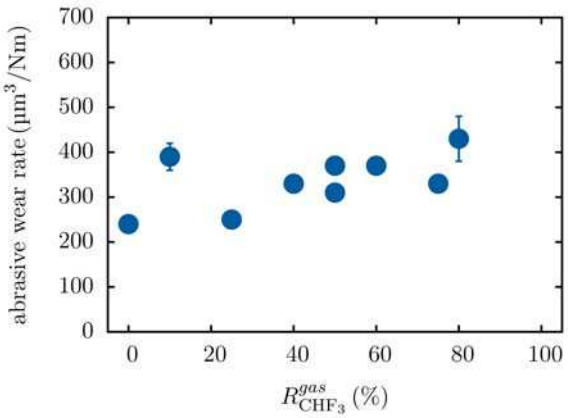

Fig. 7. Abrasive wear rate of the films after 6 min with a 1:3 suspension of alumina particles 1 μm in diameter in glycerin, with a load of 0.54 N

3. Modification by surface structuring

3.1 Structuring strategies

Tribological measurements of patterned surfaces involve the use of macroscopic probes, in order to sufficiently average the effect of the structures. Therefore, large-area capable patterning techniques are required. Here, we report on the tribological properties of samples prepared by colloidal lithography (bottom-up approach), although other structures have also been prepared by electron beam lithography (top-down).

Colloidal lithography is a fast, cost-efficient technique able to produce periodic nanometric features in large-scale (up to some centimeters or more) with high quality. The technique consists on the arrangement of particles on a substrate so that they can be used as a template/mask for subsequent etching (see figure 8). Although CL is less versatile than EBL or other lithographic techniques, regarding non-periodic patterns, the reduction of time and resources for the production of large-area periodic nanopatterns represents important advantages for certain applications or fields such as photonic crystals, [López, 2003] thermophotovoltaics [Mao & Ye, 2010] or optical biosensors [Dorfner et al., 2009]. The differences in the structuring produced by ion beam etching with different angles have been studied as a method for nanoimprint mold fabrication [Portal et al., 2009].

On the other hand, the realization of sub-100 nm features in large areas with e-beam lithography (EBL) requires the stitching of several exposure fields. Proper alignment of the fields is complicated and, depending on how critical good stitching is, specific design of the equipment is required. Laser interferometer driven stages provide state-of-the-art stitching, but even with them a small thermal expansion/contraction of the sample after introduction on the e-beam writer is to be expected even for small temperature differences. This change in size can affect the stitching quality if enough time is not allowed for stabilization.

With these precautions taken into account, EBL is a suitable technique for large-area patterning, although expensive equipment is required, and patterning is slow. Other faster techniques such as those based on light (X-Ray or extreme UV lithography) can be much faster but also even more expensive.

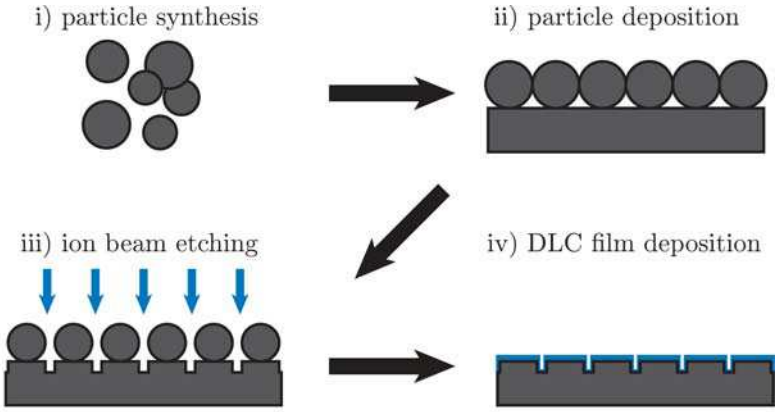

Fig. 8. Fabrication process of DLC films with patterned surface: i) Synthesis of silica particles; ii) Particle deposition by Langmuir-Blodgett (colloidal template); iii) Pattern transfer to the substrate surface (Ar+ beam etching); iv) DLC film deposition on the patterned substrate.

In the following subsection we report on the friction and wear behavior of structured DLC films.

3.2 Friction and wear of patterned films

As described above, surface structuring leads to a variation in surface properties, such as adhesion, wear resistance, friction, wettability and gas adsorption. Textured coatings must show superior tribological properties in applications leading to strong interfacial interactions like nanoimprint molds, self-cleaning surfaces, MEMS and data storage devices. A series of DLC samples with modified surface topographies were prepared by colloidal lithography following the procedure schematized in figure 8. After DLC deposition on the patterned c-Si samples, the surface topography was studied by scanning electron microscopy (SEM) and atomic force microscopy (AFM), and friction tests were performed on them.

Coefficient of friction was measured by means of a nanotribometer from CSM Instruments in ball-on-disk configuration. The ST-117 cantilever was used with a WC ball 3 mm in diameter and 100 mN of load was applied on the sample, performing circular tracks of 1.6 mm in diameter at 1 mm/s during 6250 cycles. The measurements were carried out in a nitrogen atmosphere at 40% relative humidity, which was controlled by means of a PID system equipped with a water bubbler. More details can be found elsewhere [Rubio-Roy et al., 2009].

SEM micrographs in figure 9 show the surface morphology of DLC films deposited on substrates that underwent different times of ion beam etching. In these samples, film thickness is of the order of the pit depth after etching, i.e. 50 nm. The shadowing effect of the silica particles (SP) led to the formation of a pillar network. The substrate was only etched at the interstices of the 2-D crystal monolayer, which acted as a sacrificial template during the substrate lithography. Thus, the resulting topography reproduced the pattern of the CL template, where the pillar top coincides with the substrate region protected by the particle. In general, the pillar height increases with etching time. However, the surface structure

substantially changes when the etching time surpasses a threshold between 30 and 45 min. According to figure 9, the pillar network vanished with 45 min of substrate etching. At this etching time, the SP could not be removed from the patterned c-Si probably due to an effect of particle implantation. Furthermore, when the IBE is performed during 60 min, the SP are totally etched, i.e. the particle monolayer that constitutes the etching mask is removed by the bombarding ions and only the resulting rough surface remains.

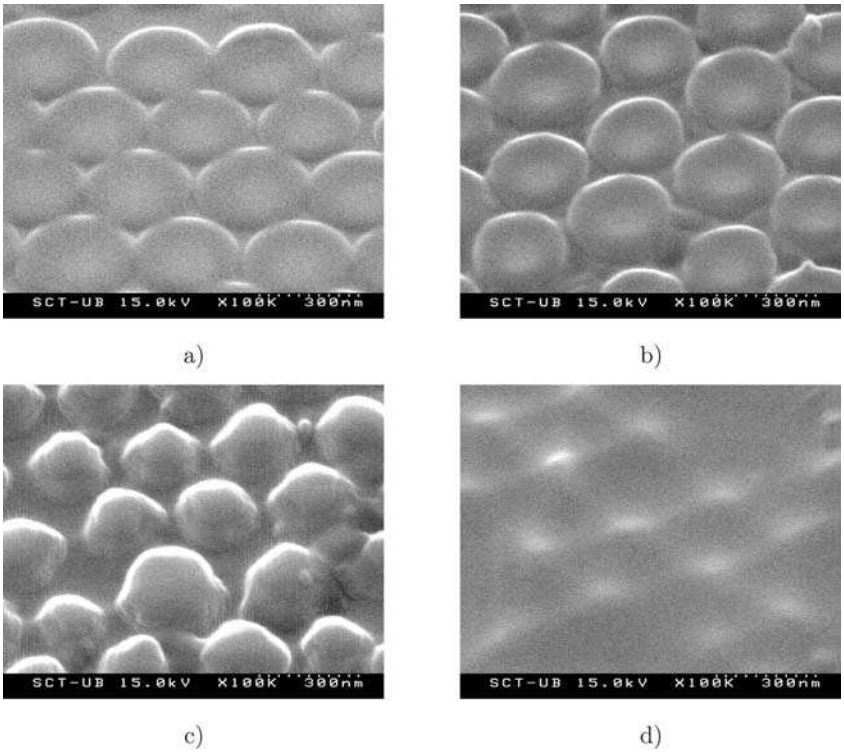

Fig. 9. SEM micrographs of DLC-coated (50 nm) substrates patterned by colloidal lithography for different etching times: (a) 15, (b) 30, (c) 45 and (d) 60 min. [Corbella et al., 2010]

Figure 10a shows the evolution of coefficient of friction of a flat DLC film measured with the nanotribometer. This parameter increased gradually from 0.12 to 0.23 passing through different stages. As reported elsewhere, the curve is divided into three sections [Corbella et al., 2009b]: run-in period, transition regime and steady state. The variations in the first stage are ascribed to surface ploughing and mechanically induced desorption of hydrogen. During the transient regime, surface modification conformal to the ball shape takes place, as well as interactions with wear particles. Finally a steady state is achieved around cycle #4000. This scenario changes in the case of structured DLC samples (figures 10b and 10c). The coefficient of friction, which is already stabilized around or prior to cycle #1000, ranges between 0.17 and 0.20. The measured samples achieved lower and more stable values than in the flat DLC coating. Spikes in the friction coefficient (not shown in figure 10 due to data

smoothing) could come from momentary interactions of the wear particles with the ball of the nanotribometer. These particles, which are debris removed from the sample during the tests, contribute to enhance the friction via several mechanisms, as for instance dragging, ploughing or adhesion.

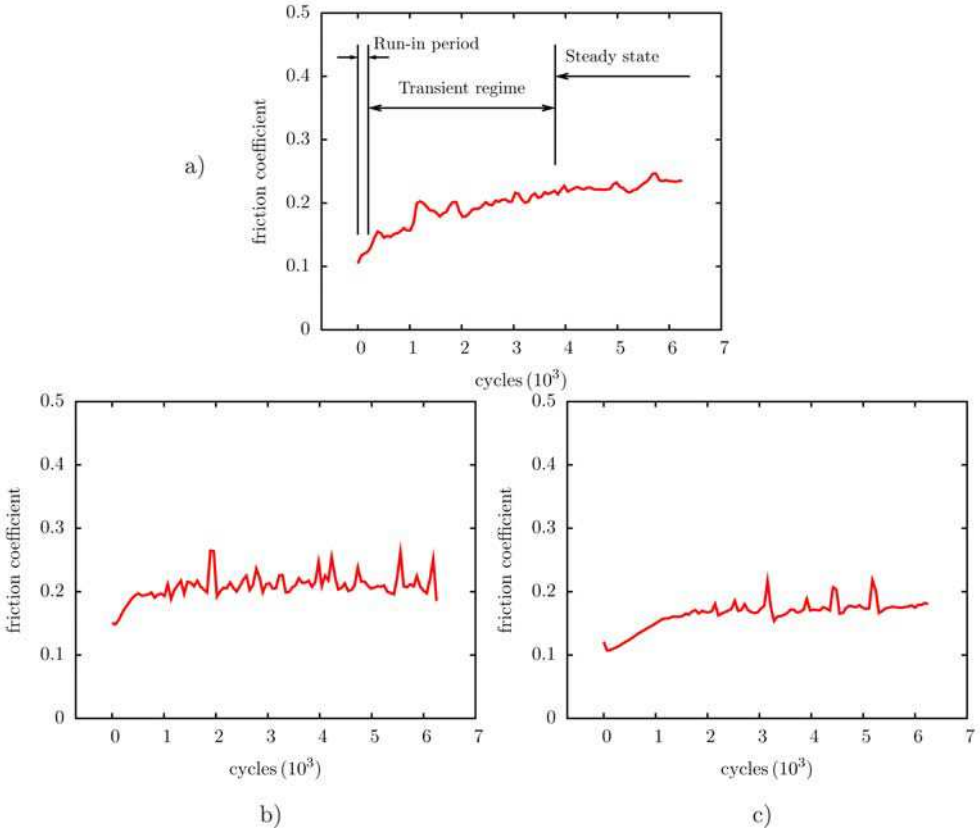

Fig. 10. Evolution of coefficient of friction of DLC films deposited on a) flat, b) 15 min, and c) 30 min etched substrates. In the first plot, we have indicated the run-in period, transition region and steady state.

The wear effects on surface structure due to nanotribometry are evidenced by the morphological changes of the pillars located on the wear track. These pillars lost the concave ending observed in figure 9. Thus, the pillar edges constitute the initial contact region between the ball and sample surface. Since the pillars are progressively worn by the WC ball, the friction increases until the pillar top becomes flat. From this moment onwards, the coefficient of friction of the patterned DLC stabilizes into the values shown in figure 10. The wear rate was quantified from AFM profilometry of the volume removed by the ball. A value of 10^{-7} $mm^3N^{-1}m^{-1}$ was measured for flat DLC from the wear track left by the nanotribometer, whereas textured DLC exhibited a rate 10 times higher. The reduced contact area in the case of a patterned surface with respect to a flat surface may cause this

increase in wear rate. Therefore, more robust structures are required to improve the wear resistance.

The coefficient of friction of the sample etched during 15 min (figure 10b) is reduced 13% with respect to flat DLC, whereas the reduction corresponding to the sample etched for 30 min is 26% (figure 10c). This behavior is in agreement with the results from Jung et al., where the role of asperity size on friction was discussed [Jung et al., 2006]. The reduction in the stable values of coefficient of friction may be ascribed to the trapping effect of the pits defined by the micro-pillars. These interstices could store the wear particles generated during the tribological tests. The effect of these wear particles on friction force is thus alleviated in comparison with systems formed by lower pillars [Dumitru et al., 2003]. Also, the higher pillars lead to a weaker interaction with the sample due to the larger distance between the WC ball and the base surface. This explanation supports the monotonic reduction in friction coefficient as the pillar height increases. In this scenario, the preparation of a non-close-packed 2D crystal could give place to weaker friction forces due to a more important particle trapping. A more complete modeling of the tribological phenomena at the nanoscale should also account for the elastic response of the micro-pillars to the friction force.

4. References

Abbas, G.A.; Roy, S.S.; Papakonstantinou, P. & McLaughlin, J.A. (2005) Structural investigation and gas barrier performance of diamond-like carbon based films on polymer substrates. *Carbon* 43, 303-309

Ager, J.W.; Anders, S.; Brown, I.G.; Nastasi, M. & Walter, K.C. (1997) Multilayer hard carbon films with low wear rates. *Surface and Coatings Technology* 91, 91-94

Aisenberg, S. & Chabot, R. (1971) Ion-beam deposition of thin films of diamondlike carbon. *Journal of Applied Physics* 42, 2953-2958

Bahl, R.; Vedawyas, M.; Patel, D.; Kumar, A. & Shamsuzzoha, M. (2000) Evaluation of mechanical properties of DLC-TiC microlaminate coatings, In: *Thin Films-Stresses and Mechanical Properties VIII*, Vinci, R.; Kraft, O.; Moody, N.; Besser, P. & Shaffer, E. (Ed.), 331–336, Materials Research Society.

Bertran, E.; Corbella, C.; Pintol, A.; Vives, M. & Andújar, J.L. (2003) Comparative study of metal/amorphous-carbon multilayer structures produced by magnetron sputtering. *Diamond and Related Materials* 12, 1008-1012

Bhushan, B. (1999) Chemical, mechanical and tribological characterization of ultra-thin and hard amorphous carbon coatings as thin as 3.5 nm: recent developments. *Diamond and Related Materials* 8, 1985-2015

Casiraghi, C.; Ferrari, A.C.; Ohr, R.; Chu, D. & Robertson, J. (2004) Surface properties of ultra-thin tetrahedral amorphous carbon films for magnetic storage technology. *Diamond and Related Materials 13*, 1416-1421

Chen, J.S.; Lau, S.P.; Sun, Z.; Chen, G.Y.; Li, Y.J.; Tay, B.K. & Chai, J.W. (2001) Metal-containing amorphous carbon films for hydrophobic application. *Thin Solid Films* 398-399, 110-115

Chen, L.Y. & Hong F.C.N. (2003) Diamond-like carbon nanocomposite films. *Applied Physics Letters* 82, 3526-3528

Chhowalla, M. (2003), In: *Properties of Amorphous Carbon*, Silva S.R.P. (Ed.), INSPEC, The Institution of Electrical Engineers

Corbella, C.; Bialuch, I.; Kleinschmidt, M. & Bewilogua, K. (2008) Modified DLC coatings prepared in a large-scale reactor by dual microwave/pulsed-DC plasma-activated chemical vapour deposition. *Thin Solid Films* 517(3), 1125-1130

Corbella, C.; Echebarria, B.; Ramírez-Piscina, L.; Pascual, E.; Andújar, J.L. & Bertran, E. (2009a) Growth kinetics of nanometric dendrites in metal-carbon thin films. *Acta Mater* 57(17), 4948-4956

Corbella, C.; Rubio-Roy, M.; Bertran, E.; Polo, M.C.; Pascual, E. & Andújar, J.L. (2009b) Low friction and protective diamond-like carbon coatings deposited by asymmetric bipolar pulsed plasma. *Diamond and Related Materials* 18(5-8), 1035-1038

Corbella, C.; Portal, S.; Rubio-Roy, M.; Vallvé, M.A.; Ignés-Mullol, J.; Bertran, E. & Andújar, J.L. (2010) Surface structuring of diamond-like carbon films by colloidal lithography with silica sub-micron particles. *Diamond and Related Materials* 19(7-9), 1124-1130

Dearnaley, G. & Arps, J. H. (2005) Biomedical applications of diamond-like carbon (DLC) coatings: A review. *Surface and Coatings Technology* 200, 2518-2524

Dimigen, H.; Hübsch, H. & Memming, R. (1987) Tribological and electrical properties of metal-containing hydrogenated carbon films. *Applied Physics Letters* 50, 1056-1058

Donnet, C. (1998) Recent progress on the tribology of doped diamond-like and carbon alloy coatings: a review. *Surface and Coatings Technology* 100-101, 180–186

Dorfner, D.; Zabel, T.; Hürlimann, T.; Hauke, N.; Frandsen, L.; Rant, U.; Abstreiter, G. & Finley, J. (2009) Photonic crystal nanostructures for optical biosensing applications. *Biosensors and Bioelectronics* 24(12), 3688–3692

Dumitru, G.; Romano, V.; Weber, H.P.; Pimenov, S.; Kononenko, T.; Hermann, J.; Bruneau, S.; Gerbig, Y. & Shupegin, M. (2003) Laser treatment of tribological DLC films. *Diamond and Related Materials* 12(3-7), 1034-1040

Endo, K. & Tatsumi, T. (1995) Fluorinated amorphous carbon thin films grown by plasma enhanced chemical vapor deposition for low dielectric constant inter-layer dielectrics. *Journal of Applied Physics* 78(2), 1370–1372

Erdemir, A. (2001) The role of hydrogen in tribological properties of diamond-like carbon films. *Surface and Coatings Technology* 146-147, 292–297

Erdemir, A. & Donnet, C. (2006) Tribology of diamond-like carbon films: recent progress and future prospects. *Journal of Physics D: Applied Physics* 39(18), R311

Fallon, P. J.; Veerasamy, V. S.; Davis, C. A.; Robertson, J.; Amaratunga, G. A. J.; Milne, W. I. & Koskinen, J. (1993) Properties of filtered-ion-beam-deposited diamondlike carbon as a function of ion energy. *Physical Review B* 48(7), 4777–4782

Ferrari, A. C. & Robertson J. (2000) Interpretation of Raman spectra of disordered and amorphous carbon. *Physical Review B* 61(20), 14095–14107

Ferrari, A. C.; Rodil, S. E.; Robertson, J. & Milne, W. I. (2002) Is stress necessary to stabilise sp^3 bonding in diamond-like carbon? *Diamond and Related Materials*, 11(3-6), 994–999

Gahlin, R.; Larsson, M. & Hedenqvist, P. (2001) Me-C:H coatings in motor vehicles. *Wear* 249, 302-309

Gee, M. G.; Gant, A.; Hutchings, I.; Bethke, R.; Schiffman, K.; Van Acker, K.; Poulat, S.; Gachon, Y. & von Stebut, (2003) J. Progress towards standardisation of ball cratering, *Wear* 255(1-6), 1-13

Gilmore, R. & Hauert, R. (2001) Control of the tribological moisture sensitivity of diamond-like carbon films by alloying with F, Ti or Si. *Thin Solid Films* 398-399, 199–204

Goldstein, J. I.; Newbury, D. E.; Echlin, P.; Joy, D. C.; Fiori, C. & Lifshin, E. (1992) *Scanning Electron Microscopy and X-Ray Microanalysis*. Plenum Press, ISBN 0-306-44175-6

Gonon, P. & Sylvestre, A. (2002) Dielectric properties of fluorocarbon thin films deposited by radio frequency sputtering of polytetrafluoroethylene. *Journal of Applied Physics* 92(8), 4584–4589

Grill, A. (1999) Diamond-like carbon: state of the art. *Diamond and Related Materials* 8(2-5), 428–434

Grill, A. (2003) Diamond-like Carbon coatings as biocompatible materials – an overview. *Diamond and Related Materials.* 12, 166-170

Grischke, M.; Bewilogua, K.; Trojan, K. & Dimigen, H. (1995) Application-oriented modifications of deposition processes for diamond-like-carbon-based coatings. *Surface and Coatings Technology* 74-75, 739–745

Grischke, M.; Hieke, A.; Morgenweck, F. & Dimigen, H. (1998) Variation of the wettability of DLC-coatings by network modification using silicon and oxygen. *Diamond and Related Materials* 7(2-5), 454-458

Guerino, M.; Massi, M. & Mansano, R. (2007) The influence of nitrogen and fluorine on the dielectric constant of hydrogenated amorphous carbon (a-C:H) films. *Microelectronics Journal* 38(8-9), 915–918

Hauert, R. & Patscheider, J. (2000) From alloying to nanocomposites – Improved performance of hard coatings. *Advanced Engineering Materials* 2, 247-259

Hauert, R. (2004) An overview on the tribological behavior of diamond-like carbon in technical and medical applications. *Tribology International* 37, 991-1003

Heimberg, J. A.; Wahl, K. J.; Singer, I. L. & Erdemir, A. (2001) Superlow friction behavior of diamond-like carbon coatings: Time and speed effects. *Applied Physics Letters* 78(17), 2449–2451

Jacobsohn, L. G.; Franceschini, D. F.; da Costa, M. E. H. M. & Freire, J. F. L. (2000) Structural and mechanical characterization of fluorinated amorphous-carbon films deposited by plasma decomposition of CF_4–CH_4 gas mixtures. *Journal of Vacuum Science & Technology A: Vacuum, Surfaces, and Films* 18(5), 2230–2238

Jiang, M. & Ning, Z. (2006) Influence of deposition pressure on the structure and properties of fluorinated diamond-like carbon films prepared by RF reactive magnetron sputtering. *Surface and Coatings Technology* 200(12-13), 3682–3686

Jiang, W. F.; Diao, D. F.;(2010) The Critical Conditions for Tribo-Demagnetization of Perpendicular Magnetic Recording Disk Under Sliding Contact. *Journal of Tribology* 132(2), 021901

Johnston, S.V. & Hainsworth, S.V. (2005) Effect of DLC coatings on wear in automotive applications. *Surface Engineering* 21, 67-71

Jung, Y.C. & Bhushan, B. (2006) Contact angle, adhesion and friction properties of micro- and nanopatterned polymers for superhydrophobicity. *Nanotechnology* 17, 4970-4980

Kaukonen, H. P. & Nieminen, R. M. (1992) Molecular-dynamics simulation of the growth of diamondlike films by energetic carbon-atom beams. *Physical Review Letters* 68(5), 620–623

Kawasaki, D.; Tsuchimura, D.; Choi, W.; Iseri, Y.; Ando, T. & Tomokage, H. (2004). Scanning probe field emission current measurements on diamond-like carbon films treated by reactive ion etching. *Journal of Physics: Condensed Matter* 16(2), S301

Kessels, W. M. M.; Gielen, J. W. A. M.; de Sanden, M. C. M. V.; Ijzendoorn, L. J. V.; Dekempeneer, E. H. A. & Schram, D. C. (1998) A model for the deposition of a-C:H using an expanding thermal arc. *Surface and Coatings Technology* 98(1-3), 1584–1589

Kim, T.Y.; Bialuch, I.; Bewilogua, K.; Oh, K.H. & Lee, K.R. (2007) Wetting behaviours of a-C:H:Si:O film coated nano-scale dual rough surface. *Chemical Physics Letters* 436(1-3), 199-203

Kiuru, M.; Alakoski, E.; Tiainen, V. M.; Lappalainen, R. & Anttila, A. (2003) Tantalum as a buffer layer in diamond-like carbon coated artificial hip joints. *Journal of Biomedical Materials Research Part B: Applied Biomaterials*, 66B(1), 425–428

Ko, H.P.; Kim, S.; Kim, J.S.; Kim, H.J. & Yoon, S.J. (2005) Wear and dynamic properties of piezoelectric ultrasonic motor with frictional materials coated stator. *Materials Chemistry and Physics* 90, 391-395

Koidl, P.; Wild, C.; Dischler, B.; Wagner, J. & Ramsteiner, M. (1990) Plasma deposition, properties and structure of amorphous hydrogenated carbon films. *Materials Science Forum* 52, 41–70

Korotkov, R.; Goff, T. & Ricou, P. (2007) Fluorination of polymethylmethacrylate with SF6 and hexafluoropropylene using dielectric barrier discharge system at atmospheric pressure. *Surface and Coatings Technology* 201(16-17), 7207–7215

Lampe, Th.; Eisenberg, S. & Rodríguez Cabeo, E. (2003) Plasma surface engineering in the automotive industry – trends and future prospective. *Surface and Coatings Technology* 174-175, 1-7

Lee, K. R.; Eun, K. Y.; Kim, I. & Kim, J. (2000) Design of W buffer layer for adhesion improvement of dlc films on tool steels. *Thin Solid Films* 377-378, 261–268

Li, K. Y.; Zhou, Z. F.; Bello, I.; Lee, C. S. & Lee S. T. (2005) Study of tribological performance of ECR-CVD diamond-like carbon coatings on steel substrates: Part 1. The effect of processing parameters and operating conditions. *Wear* 258(10), 1577–1588

Lifshitz, Y.; Kasi, S. R. & Rabalais, J. W. (1989) Subplantation model for film growth from hyperthermal species: Application to diamond. *Physical Review Letters* 62(11), 1290–1293

Lifshitz, Y.; Kasi, S. R.; Rabalais, J. W. & Eckstein, W. (1990) Subplantation model for film growth from hyperthermal species. *Physical Review B* 41(15), 10468–10480

Lifshitz, Y.; Lempert, G. D. & Grossman, E. (1994) Substantiation of subplantation model for diamondlike film growth by atomic force microscopy. *Physical Review Letters* 72(17), 2753–2756

Logothetidis, S.; Charitidis, C.; Gioti, M.; Panayiotatos, Y.; Andrea, M. & Kautek, W. (2000) Comprehensive study on the properties of multilayered amorphous carbon films. *Diamond and Related Materials* 9, 756-760

López, C. (2003) Materials aspects of photonic crystals. *Advanced Materials* 15(20), 1679–1704

Ma, W. J.; Ruys, A. J.; Mason, R. S.; Martin, P. J.; Bendavid, A.; Liu, Z.; Ionescu, M. & Zreiqat, H. (2007) DLC coatings: Effects of physical and chemical properties on biological response. *Biomaterials* 28, 1620-1628

Mao, L. & Ye, H. (2010) New development of one-dimensional Si/SiO_2 photonic crystals filter for thermophotovoltaic applications. *Renewable Energy* 35(1), 249–256

Martin, P. J; Filipczuk, S. W.; Netterfield, R. P.; Field, J. S.; Whitnall, D. F. & McKenzie, D. R. (1988) Structure and hardness of diamond-like carbon films prepared by arc evaporation. *Journal of Materials Science Letters* 7(4), 410–412

McKenzie, D. R.; Muller, D. & Pailthorpe, B. A. (1991) Compressive-stress-induced formation of thin-film tetrahedral amorphous carbon. *Physical Review Letters* 67(6), 773– 776

Miyamoto, T.; Kaneko, R. & Miyake, S. (1991) Tribological characteristics of amorphous carbon films investigated by point contact microscopy. *Journal of Vacuum Science & Technology B* 9(2), 1336–1339

Miyazawa, T.; Misawa, S.; Yoshida, S.; & Gonda, S. (1984) Preparation and structure of carbon film deposited by a mass-separated C+ ion beam. *Journal of Applied Physics* 55(1), 188–193

Morrison, N. A.; Rodil, S. E.; Ferrari, A. C.; Robertson, J. & Milne, W. I. (1999) High rate deposition of ta-C:H using an electron cyclotron wave resonance plasma source. *Thin Solid Films* 337(1-2), 71–73

Mountsier, T. W. & Samuels, J. A. (1998) Precursor selection for plasma deposited fluorinated amorphous carbon films. *Thin Solid Films* 332(1-2), 362–368

Ozeki, K.; Nagashima, I.; Ohgoe, Y.; Hirakuri, K. K.; Mukaibayashi, H. & Masuzawa, T. (2009) Gas barrier properties of diamond-like carbon films coated on PTFE. *Applied Surface Science* 255, 7286-7290

Peng, X.L.; Barber, Z.H. & Clyne, T.W. (2001) Surface roughness of diamond-like carbon films prepared using various techniques. *Surface and Coatings Technology* 138, 23-32

Pino, F.J.; Bertran, E.; Polo, M.C. & Andújar, J.L. (2001) Microstructural and mechanical properties of nanometric-multilayered a-CN/a-C/…/a-CN coatings deposited by rf-magnetron sputtering and nitrogen ion-beam bombardment. *Diamond and Related Materials* 10, 952-955

Polo, M.C.; Andújar, J.L.; Hart, A.; Robertson, J. & Milne, W.I. (2000) Preparation of tetrahedral amorphous carbon films by filtered cathodic vacuum arc deposition. *Diamond and Related Materials* 9(3-6), 663-667

Portal, S.; Rubio-Roy, M.; Corbella, C.; Vallvé, M.; Ignes-Mullol, J. & Bertran, E. (2009) Influence of incident ion beam angle on dry etching of silica sub-micron particles deposited on Si substrates. *Thin Solid Films* 518(5), 1543–1548

Randhawa, H. (1988) Cathodic arc plasma deposition technology. *Thin Solid Films* 167(1-2), 175-185

Robertson, J. (1993) Deposition of diamond-like carbon. *Philosophical Transactions of the Royal Society of London. Series A: Physical and Engineering Sciences* 342(1664), 277–286

Robertson, J. (2002) Diamond-like amorphous carbon. *Materials Science and Engineering R* 37, 129-281

Rodil, S.E. (2000) PhD Thesis: *Preparation and characterization of carbon nitride thin films*, University of Cambridge, Cambridge.

Roy, R. K.; Choi, H. W.; Park, S. J. & Lee, K. R. (2007) Surface energy of the plasma treated Si incorporated diamond-like carbon films. *Diamond and Related Materials*, 16(9), 1732–1738

Roy, R. K. & Lee, K. R. (2007) Biomedical Applications of Diamond-Like Carbon Coatings: A Review. *Journal of Biomedic Materials Research B: Applied Biomaterials* 83, 72-84

Rubio-Roy, M.; Corbella, C.; García-Céspedes, J.; Polo, M.C.; Pascual, E.; Andújar, J.L. & Bertran, E. (2007a) Diamondlike carbon films deposited from graphite target by asymmetric bipolar pulsed-DC magnetron sputtering. *Diamond and Related Materials* 16(4-7), 1286-1290

Rubio-Roy, M.; Bertran, E.; Pascual, E.; Polo, M.C. & Andújar, J.L. (2007b) Fluorinated DLC deposited by pulsed-DC plasma for antisticking surface applications. *Diamond and Related Materials* 17(7-10), 1728-1732

Rubio-Roy, M.; Corbella, C.; Bertran, E.; Portal, S.; Polo, M.; Pascual, E. & Andújar, J. (2009) Effects of environmental conditions on fluorinated diamond-like carbon tribology. *Diamond and Related Materials* 18(5-8), 923–926

Rusli; Yoon, S.F. & Huang, Q.F. (2003), Hydrogenated a-C optical coatings, In: *Properties of Amorphous Carbon*, Silva S.R.P. (Ed.), INSPEC, The Institution of Electrical Engineers

Sanders, D.M. & Anders, A. (2000) Review of cathodic arc deposition technology at the start of the new millennium. *Surface and Coatings Technology* 133-134, 78-90

Scheibe, H.J. & Schultrich, B. (1994) DLC film deposition by laser-arc and study of properties. *Thin Solid Films* 246(1-2), 92–102

Schvartzman, M. & Wind, S. J. (2009) Plasma fluorination of diamond-like carbon surfaces: mechanism and application to nanoimprint lithography. *Nanotechnology* 20(14), 145306

Silva, S.; Carey, J.; Khan, R.; Gerstner, E. & Anguita, J. (2002) Amorphous carbon thin films, In: *Handbook of Thin Films*, Nalwa, H. S. (Ed.), 403–506. Academic Press, ISBN 978-0-12-512908-4, Burlington.

Silva, S.R.P. (2003), Microstructure of a-C, In: *Properties of Amorphous Carbon*, Silva S.R.P. (Ed.), INSPEC, The Institution of Electrical Engineers

Simko, J. P.; Oehrlein, G. S. & Mayer, T. M. (1991) Removal of fluorocarbon residues on CF_4/H_2 reactive-ion-etched silicon surfaces using a hydrogen plasma. *Journal of The Electrochemical Society* 138(1), 277–284

Tang, G.; Ma, X.; Sun, M. & Li, X. (2005) Mechanical characterization of ultra-thin fluorocarbon films deposited by R.F. magnetron sputtering. *Carbon* 43(2), 345–350

Trippe, S. C.; Mansano, R. D.; Costa, F. M. & Silva, R. F. (2004) Mechanical properties evaluation of fluor-doped diamond-like carbon coatings by nanoindentation. *Thin Solid Films* 446(1), 85–90

Voevodin, A.A. & Donley, M.S. (1996) Preparation of amorphous diamond-like carbon by pulsed laser deposition: a critical review. *Surface and Coatings Technology* 82, 199-213

Voevodin, A.A.; Phelps, A.W.; Zabinski, J.S. & Donley, M.S. (1996) Friction induced phase transformation of pulsed laser deposited diamond-like carbon. *Diamond and Related Materials* 5, 1264-1269

Weiler, M.; Sattel, S.; Giessen, T.; Jung, K.; Ehrhardt, H.; Veerasamy, V. S. & Robertson, J. (1996) Preparation and properties of highly tetrahedral hydrogenated amorphous carbon. *Physical Review B* 53(3), 1594–1608

Winder, E. J. & Gleason, K. K. (2000) Growth and characterization of fluorocarbon thin films grown from trifluoromethane (CHF_3) using pulsed-plasma enhanced cvd. *Journal of Applied Polymer Science* 78(4):842–849